COMMUNICATION

# Porous One-Dimensional Photonic Crystals Improve the Power-Conversion Efficiency of Dye-Sensitized Solar Cells

By *Silvia Colodrero, Agustín Mihi, Leif Häggman, Manuel Ocaña, Gerrit Boschloo, Anders Hagfeldt,** and *Hernán Míguez**

Dye-sensitized solar cells (DSSCs)[1–3] combine a solid, wide-bandgap semiconductor with a liquid ionic conductor. They usually consist of one electrode made of a layer of a few micrometers of titanium dioxide nanocrystals (nc-$TiO_2$, average crystal size around 20 nm), on whose surface a dye, typically a ruthenium polypyridyl complex, is adsorbed. This nanocrystalline film is deposited onto a conductive, transparent substrate, typically indium tin oxide (ITO) or fluorinated $SnO_2$, and soaked with a redox electrolyte, typically containing $I^-/I^{3-}$ ion pairs. This electrolyte is also in contact with a counterelectrode coated with a colloidal platinum catalyst. Sunlight is harvested by the dye, producing photoexcited electrons that are injected into the conduction band of the nanocrystalline semiconductor network, and then into the conducting substrate. At the same time, the redox electrolyte reduces the oxidized dye and transports the electron-acceptor species ($I^{3-}$) to the counterelectrode.[4] Many different modifications of the originally proposed cell have been made in order to improve its performance, most of them based on using different semiconductors,[5] dyes[6] or ionic conductors,[7] or on alterations of its nanostructure.[8–10] In many cases a change of the cell constituents gives rise to an improvement in the short-circuit current, but causes at the same time a decrease in the open-circuit voltage and vice versa. This is due to the sensibility of the charge-transport and recombination dynamics to any alteration of the nature of the interfaces present in the cell.[11]

One way to enhance the cell efficiency without affecting the delicate kinetic balance between charge separation and recombination is to modify the optical design of the cell in order to improve its light-harvesting efficiency (LHE) or absorptance. Reflecting unabsorbed photons back into the film has proven to largely improve the incident-photon-to-current conversion efficiency (IPCE). In fact, a diffuse scattering layer of large $TiO_2$ colloids[12] is typically introduced for this specific purpose in the standard design of the cells that show the best performance, i.e., an IPCE of around 90% at the absorption maximum.[13] Unfortunately, some of the most successful approaches developed to improve the LHE in silicon photovoltaic devices, which are based on the implementation of coherent scattering devices such as highly reflecting distributed Bragg reflectors,[14] surface gratings,[15] or a combination of both,[16] cannot be easily realized in liquid–semiconductor heterojunction cells. First, the need for an electrical contact between the electrolyte and the sensitized semiconductor slab forces any potential back reflector to be porous in order to allow a proper flow of the liquid conductor through it. Second, the processing of these cells involves deposition of solid layers from colloidal suspensions, which complicates the implementation of quality optical components in the device. Recently, an interesting new route was opened by coupling inverse opals to dye-sensitized nc-$TiO_2$ films. In doing so, the IPCE[17] was shown to increase with respect to that of a standard reference cell. However, the observation of a higher IPCE does not necessarily imply better performance. Although valid as a proof of concept, this experiment provided no information on the actual power-conversion efficiency, $\eta$, of the device, which is the ultimate parameter for evaluating its performance. Thick inverse opals (5–10 μm thick) are very likely to have a deleterious effect on charge transport and recombination through the cell, which results in a significant reduction in both the open-circuit photovoltage and the photocurrent in real operation conditions.

Herein, a device for solar-energy conversion is introduced in which a porous and highly reflecting 1D photonic crystal (1D PC) is coupled to a dye-sensitized nc-$TiO_2$ electrode. This coherent mirror is made by the deposition of alternate layers of nanoparticles of different compositions by spin-coating.[18] Its porous mesostructure allows the electrolyte to flow through it and soak the electrode without interfering with the charge transport through the cell. With a thickness of just half a micrometer, the PC is able to efficiently localize incident light within the nc-dyed $TiO_2$ electrode in a targeted wavelength range. Average power-conversion efficiencies are improved to between 15 and 30% of the reference value attained for standard electrodes. The photogenerated current is greatly improved without altering the open-circuit voltage of the cell. Furthermore, the transparency of the cell, one of its added values, remains intact, contrary to what happens when scattering layers are employed to improve light harvesting.

[*] Dr. H. Míguez, S. Colodrero, Dr. A. Mihi, Dr. M. Ocaña
Instituto de Ciencia de Materiales de Sevilla
Consejo Superior de Investigaciones Científicas
Américo Vespucio 49, 41092 Sevilla (Spain)
E-mail: hernan@icmse.csic.es
Dr. L. Häggman, Dr. G. Boschloo, Prof. A. Hagfeldt
Department of Chemistry
Center of Molecular Devices
The Royal Institute of Technology
Teknikringen 30, S-100 44 Stockholm (Sweden)

DOI: 10.1002/adma.200703115

ADVANCED MATERIALS



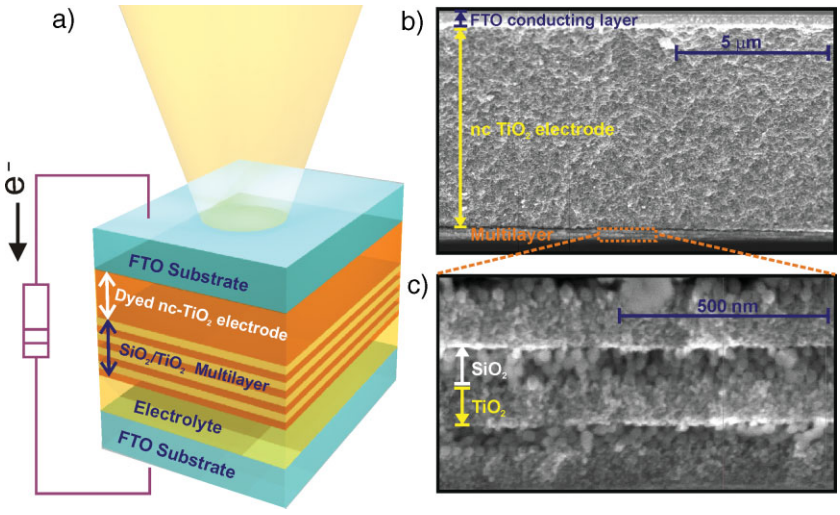


**Figure 1.** Design and microstructure of a DSSC coupled to a porous nanoparticle-based 1D PC. a) Scheme of the solar cell based on the 1D PC exposed to frontal illumination. b) FESEM image showing a cross-section of a dye-sensitized nc-$TiO_2$ electrode (total thickness indicated by the vertical yellow line) onto which a $TiO_2$–$SiO_2$ nanoparticle multilayer has been deposited (bottom of the image). c) Magnified view of the silica (spherical particles) and titania (smaller crystallites) layers composing the 1D PC.

Figure 1 displays a scheme and field emission scanning electron microscopy (FESEM) images of a cross-section of the DSSC presented in this work. The nanoparticle multilayer is periodic with a period of a few hundred nanometers and porous at the mesoscale, as can be seen in the FESEM images. The thickness of these layers is controlled through either the concentration of the precursor suspension (typically between 1 and 5 wt. %) or the rotation speed of the substrate (typically between 100 and 150 revolutions per second (rps)) during the spin-coating process. Typical values achievable are in the range 5–100 nm, although the minimum film thickness varied as a function of the particle size in suspension and its ease of dispersion. The nanoparticle multilayer behaved as a 1D PC (i.e., a distributed Bragg reflector), which provided the cell with a brilliant metallic reflection whose color could be tuned by varying the thickness of the layers forming the periodic nanostructure. This can be readily seen in the photographs shown in Figure 2, in which the appearance of a reference cell (Fig. 2a) and the same cell including two different PCs (Fig. 2b,c) under perpendicular illumination are shown. The effect of the PC is to efficiently localize incident radiation within the dye-sensitized nanocrystalline titania electrode in a specific wavelength range determined by the spectral width of its photonic bandgap, which is responsible for the colored reflection observable with the naked eye. Thus, the multilayer can be devised to present a Bragg peak that matches the absorption band of the ruthenium dye but has no effect on longer wavelengths, leaving the transparency of the cell unaltered. This is demonstrated in Figure 2d, in which the optical transmission spectra of a reference DSSC with a 7.5 μm thick titania electrode is shown (black curve) together with the spectra of two other cells possessing the same electrode coupled to PCs with different lattice parameters (green and red curves). In all cases, the multilayer structure was created by stacking six alternate layers of silica and titania nanoparticles (that is, three unit cells). In order to compare the effect on cell transparency with that of other scattering layers usually employed, the optical transmission spectrum of a DSSC made of a titania electrode coupled to a porous diffuse scattering layer of large titania nanoparticles (average size 130 nm) is also plotted as a black dashed line in Figure 2d. It can be clearly seen that the transparency of the PC-based cells in the visible range of the electromagnetic spectrum is very similar to that of the reference cell. The cell made by including a diffuse scattering layer has, however, completely lost this transparency, which is a direct consequence of the lack of spectral selectiveness of the incoherent scattering by slurries with a wide particle-size distribution.

The effect of selective light trapping, caused by the optical coupling of the PCs and absorbing slabs,[19,20] on the power-conversion efficiency of the cell, was analyzed by measuring the photocurrent-density–voltage ($J$–$V$) curves under simulated sunlight radiation of 1000 W $m^{-2}$ intensity. Results for DSSCs with a 7.5 μm thick titania electrode are shown in Figure 3, where black circles correspond to the reference cell, and green triangles and red diamonds correspond to cells with the exact same electrode but coupled to 1D PCs with lattice parameters of $120 \pm 10$ and $160 \pm 10$ nm, respectively. It can be easily concluded from these $J$–$V$ curves that the effect of the PC is to largely improve $J$, while leaving the open-circuit voltage, $V_{oc}$, (i.e., $V$ at $J = 0$) almost unaltered. A detailed analysis of the physical origin of this enhancement effect is out of the scope of this communication and will be presented elsewhere. Suffice it to say here that the magnitude of this effect depends on two factors. First, the spectral width and position of the photonic band gap relative to the absorption band of the ruthenium dye. A comparison of these is presented in the inset of Figure 3, which allows us to conclude that the multilayer whose photonic bandgap has a larger overlap with the absorption band of the ruthenium dye gives rise to a larger enhancement of the photocurrent. A second factor to be considered is the degree of optical coupling to the dye-sensitized electrode, which depends in turn on the thickness of that electrode, as has been theoretically proven.[21] This is because the number and spectral position of optical modes that can be supported by the electrode–PC ensemble, and for which absorption amplification will occur, varies with the thickness of the electrode. Measurements on electrodes thinner than those reported here coupled to PCs are included as Supporting Information. In all cases, please note that there is no contribution of the nc-$TiO_2$ layers that form the 1D PC to the photocurrent, since they are separated by insulating $SiO_2$ layers.

From the $J$–$V$ curves, $\eta$ was calculated using the equation $\eta = (ff \times J_{sc} \times V_{oc})/P_i$, where $ff$ is the fill factor, $J_{sc}$ is the absolute value of the current density at short circuit ($J$ at $V = 0$), $V_{oc}$ is the photovoltage at open circuit, and $P_i$ is the power density of the incident light. The efficiency increases from 3.9% in the

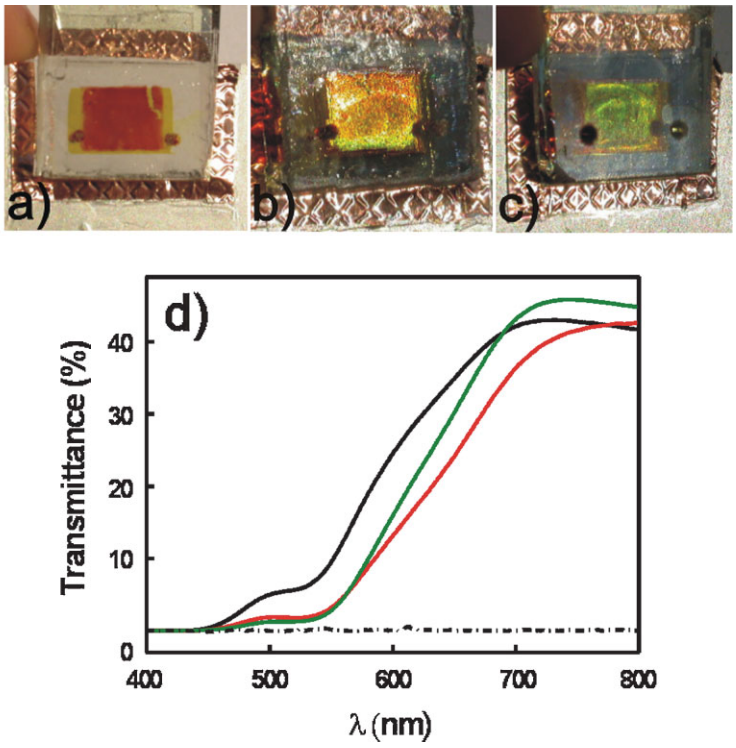


**Figure 2.** Images of different reference (a) and photonic-crystal-based (b,c) DSSCs. The different colors displayed by the cells in (b,c) arise from the different 1D PCs coupled to the same nc-$TiO_2$ electrode. The lattice parameters are $120 \pm 10$ and $160 \pm 10$ nm respectively. d) Transmittance spectra of a DSSC composed of a 7.5 μm thick titania electrode (black curve) and of the same electrode coupled to PCs with different lattice parameters (green and red curves). In all cases, the multilayer structure has been achieved by the alternate stacking of three layers of silica nanoparticles and three layers of titania nanocrystals (three unit cells). For comparison, the transmittance spectra of a DSSC made of a titania electrode coupled to a 7.5 μm thick porous diffuse scattering layer of large (average size: 130 nm) titania nanoparticles is plotted (black dashed line).

reference cell to 4.6 or 4.2% after coupling that same electrode to PCs with lattice parameters of $120 \pm 10$ or $160 \pm 10$ nm, respectively (see green and red curves in Fig. 4a). In the former case, this implies an enhancement in the efficiency of 18% with respect to that of the reference cell. This enhancement is even larger at lower incident radiation intensities, as can be seen in Figure 4a, reaching up to 31% of the reference value for 100 W $m^{-2}$. The monotonically decreasing character of the curves in Figure 4a can be explained as follows: as the incident light intensity increases so does the density of carriers, which has a negative effect on electron transport and recombination throughout the cell, giving rise to lower fill factors and, hence, to lower efficiencies. This effect is equally present in the reference and the PC-based cells. The variation of $J_{sc}$ and $V_{oc}$ with intensity of the incident radiation, shown in Figure 4b and 4c, respectively, confirms that the presence of the PC enhances the photocurrent significantly, but has a minor negative effect on the photovoltage. In the PC-based cells, $V_{oc}$ is 96% of the value attained for the reference at all radiation intensities. The linear and logarithmic dependence observed for $J_{sc}$ and $V_{oc}$, respectively, versus incident radiation intensity are in good agreement with theoretical predictions.[21,22] Regarding the fill factor, a comparison of the trends observed for the reference and the PC-based cells with incident-light intensity, shown in Figure 4d, also proves that the porous, 0.5 μm thick PC introduces a very small resistance in the cell, whose deleterious effect is more than compensated by the large increment in photocurrent the multilayer gives rise to. It should be noted that previous attempts to couple 3D PCs to dyed nc-TiO2 electrodes have yielded larger short-circuit photocurrents, but no evidence of actual improvement in $\eta$ has been reported to date.[17] This is probably due to the fact that inverted $TiO_2$ opals, usually 5–10 μm thick, introduce large resistances in the cell since the charges are forced to travel along much longer paths.

The spectral photoelectric response of the cell clearly shows the effect that coupling to a PC has on the current photogenerated in the dye-sensitized electrode. In Figure 5, the IPCE of a reference cell with a 7.5 μm thick titania electrode is compared to that of a similar cell in which the same electrode is coupled to a 1D PC with a lattice parameter of $120 \pm 10$ nm. Measurements were taken under normally incident light impinging from both sides of the cell. Under frontal illumination, light impinges first on the electrode, then on the PC. IPCEs corresponding to the reference (solid blue triangles in Fig. 5) and the PC-based (solid red circles in Fig. 5) cells were measured under these conditions. It can be seen that the PC-based cell shows a much higher short-circuit photocurrent than the reference for all the ranges in which the absorption band of the dye and the photonic bandgap of the multilayer overlaps. As previously demonstrated theoretically[20] (and as has been put into practice in thin silicon solar cells[23]), localization of light in the absorbing layer caused by the PC is responsible for longer radiation–matter interaction times, which gives rise to a higher probability of absorption, thus increasing the light harvesting. IPCEs attained under rear illumination are also included to show the strongly asymmetric response of the cell when a PC is introduced. In this experimental configuration, light impinges first on the counterelectrode, then travels through the electrolyte to reach the PC and then the dye-sensitized electrode. The open blue triangles and open red circles in Figure 5 correspond to the reference and the PC-based cell measured under these conditions, respectively. In the latter case, the PC does not localize incoming light in the dyed electrode but, contrarily, simply acts as a mirror that prevents light from reaching that layer. Consequently, the reference cell exhibits a better performance than the PC-based one under rear illumination. The much lower IPCE measured for $\lambda < 500$ nm in the case of rear illumination is due to the large optical absorption of the electrolyte in that range. It has little effect in the front-illumination configuration, since in that case light encounters the dyed electrode and the PC prior to travelling through the electrolyte.

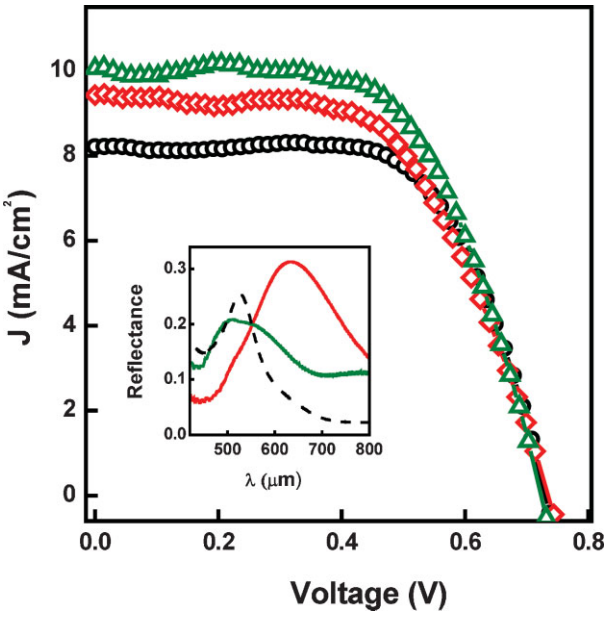


**Figure 3.** *J–V* characteristics of a 7.5 μm thick dye-sensitized nc-$TiO_2$ electrode coupled to different 1D PCs under one-sun illumination. The lattice parameters are 120 ± 10nm (open green triangles), and 160 ± 10 nm (open red diamonds). The *J–V* curve for a reference cell with the same nc-$TiO_2$ electrode is also plotted (open black circles). The inset shows the corresponding specular reflectance spectra of the PC-based solar cell (absolute units) together with the absorption spectrum of the ruthenium dye (arbitrary units).

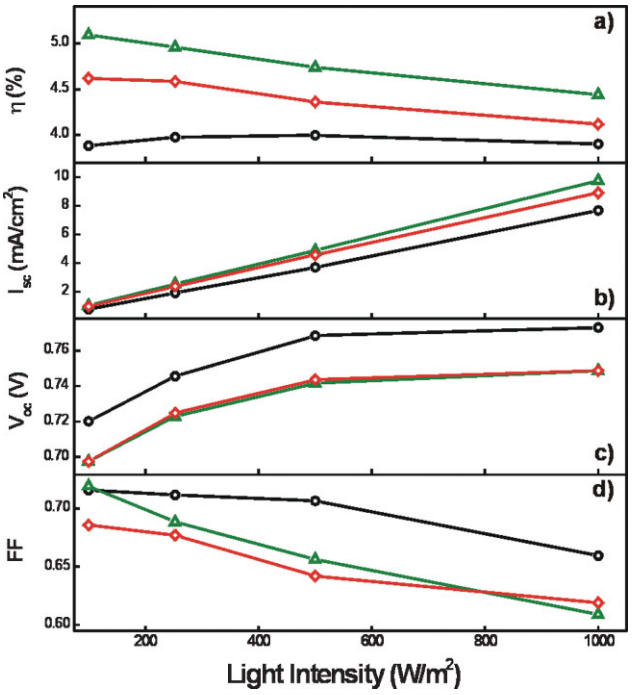


**Figure 4.** a) Efficiency $\eta$, b) short-circuit current $I_{SC}$, c) open-circuit voltage $V_{OC}$, and d) fill factor of a reference cell made of a 7.5 μm thick dye-sensitized titania electrode (open black circles) and for the corresponding solar cells with the same electrode coupled to 1D PCs with lattice parameters 120 ± 10 nm (open green triangles) and 160 ± 10nm (open red diamonds) under illumination at different light intensities.

Finally, the performance of the 1D porous PC as a light-harvesting amplifier was compared to that of diffuse scattering layers that are commonly used. For this purpose, a 7.5 μm diffuse scattering layer made of titania spheres 130 nm in diameter mixed with a paste similar to that employed to prepare the nanocrystalline titania layer was deposited onto a 7 μm thick reference electrode. A similar electrode was coupled to a 700 nm thick 1D PC with a lattice parameter of 120 ± 10 nm. In order to perform a comparison of the effect on light harvesting these different architectures have, the 7 μm thick diffuse scattering layer was electrically isolated from the dye-sensitized electrode by introducing a thin layer of silica spheres 30 nm in diameter between them. Otherwise the nanocrystalline titania paste that constitutes the diffusive layer also contributes to the photo-generated current, the overall cell behaving as if made of a 14.5 μm electrode containing scattering particles, thus preventing comparison of the light-harvesting effect. The *J–V* curves attained for this series of cells are plotted in Figure 6a. It can be clearly observed, provided that a suitable PC is chosen, that the effect of the PC on the short-circuit photocurrent is comparable to that of a diffuse scattering layer. Furthermore, the open-circuit voltage is slightly higher in the case of the PC, which might be due to its much smaller width. The values of $\eta$ attained were similar for the two approaches, as can be seen in Figure 6b. It must be mentioned that the enhancement in the case of PCs is based on the partial confinement of light of a selected frequency range within the absorbing dye-sensitized layer, which becomes an optical cavity as a result of the coupling with a photonic-bandgap material. Resonant waves confined within the dye-sensitized layer are very effectively absorbed since the matter–radiation interaction time is much longer. On the contrary, in the case of diffuse scattering layers, the increase in efficiency is based on the random and non-selective scattering of visible light in all directions. As shown in Figure 2d, transparency is preserved when PCs are used as enhancers, but not when diffuse scattering layers are employed. Although for many applications this is not an issue, some important ones, like in window modules, might significantly benefit from a method that enhances efficiency without causing loss of transparency, as occurs in the PC approach. An interesting question that arises is how these different enhancement mechanisms modify the angular response of the cell. In general, the optical response of PCs is strongly dependent on the angle of incidence of the incoming light and, therefore, the enhancement effect might vary abruptly with this parameter. In order to clarify this point, the angular response of the cells used in this comparative study (i.e., a reference cell and two cells containing the same reference electrode but coupled to a 7.5 μm thick diffuse scattering layer in one case and to a 700 nm thick PC in the other) was investigated. Measurements were taken between normal incidence and 45° in all cases. Interestingly, it was observed that the angular response of the two cells followed approximately the same trend, as shown in Figure 6b. This result, which might seem surprising, can be understood by taking into account two factors. First, before reaching the corresponding

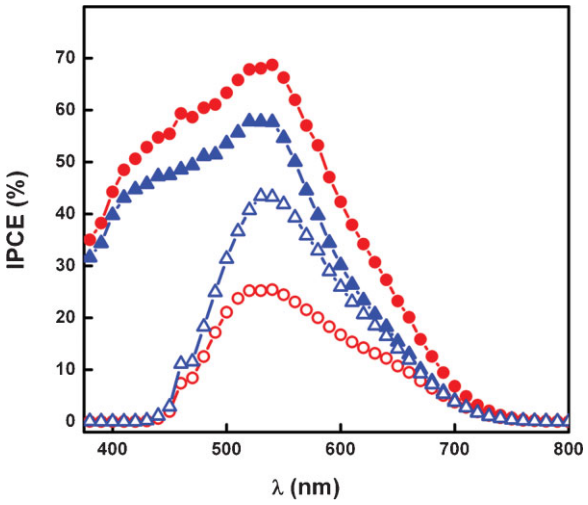


**Figure 5.** IPCE versus wavelength ($\lambda$) for a DSSC containing a 7.5 μm thick dye-sensitized $TiO_2$ electrode (solid blue triangles) and for the same electrode coupled to a PC of parameters 120 ± 10 nm (solid red circles), measured under frontal illumination. Analogous measurements collected under rear illumination are also shown (open blue triangles and open red circles, respectively).

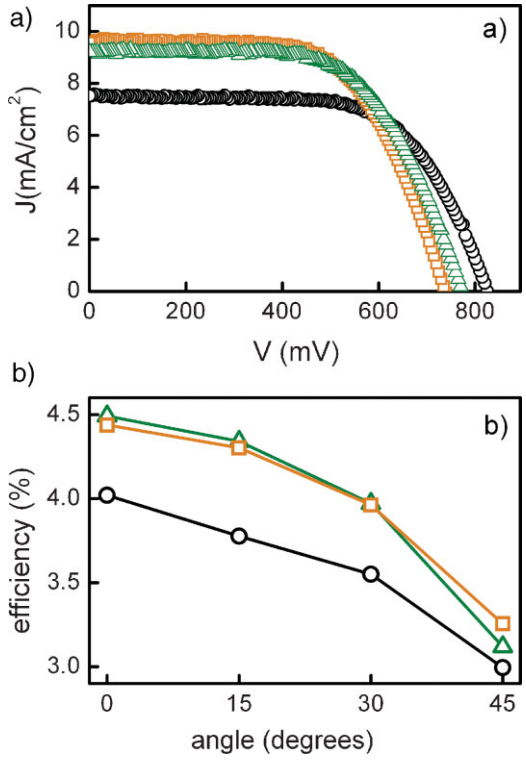


**Figure 6.** a) *J–V* characteristics of a cell made of a 7 μm thick dye-sensitized nc-$TiO_2$ electrode coupled to a 0.7 μm thick 1D PC (lattice parameter 120 ± 10 nm, open green triangles) and to a 7.5 μm thick diffuse scattering layer containing 130 nm $TiO_2$ particles (open orange squares) under one-sun illumination. The *J–V* curve for a reference cell with the same nc-$TiO_2$ electrode thickness is also plotted (open black circles). b) Variation of $\eta$ with the angle of incidence of incoming light with respect to the cell surface normal for a reference cell (open black circles) and two cells with a similar electrode coupled to a diffuse scattering layer (open orange squares) and a 1D PC (open green triangles).

scattering layer, the incident light crosses the transparent conductive oxide and the nanocrystalline titania films, undergoing consecutive refractions that cause the incident beam to move closer to the normal. The second reason behind the observed behavior is the high dielectric contrast between the nanoparticle layers that form the PC, which gives rise to a very wide photonic stop band whose angular dependence is weaker than in optical lattices of lower contrast. Due to their large spectral widths, there is a large overlap between the stop bands that exist for the different photon propagation directions and, therefore, the enhanced optical-absorption effect is less sensitive to tilting.

In conclusion, the results presented here demonstrate that nanoparticle-based porous 1D PCs implemented in a DSSC substantially enhance its power-conversion efficiency. Light absorption is amplified as a result of the localization of optical modes within the dye-sensitized electrode at photonic bandgap frequencies. These results demonstrate that colloidal chemistry approaches are suitable for implementing optical devices of high quality in DSSCs in order to improve their performance. This opens the door for the conscious optimization of the photonic design of DSSCs, as is commonly done for their silicon counterparts. PCs allow tailoring to measure the enhanced optical absorption window of the dye. This may also open the way to amplifying the absorption of other dyes with low extinction coefficients that cover other regions of the visible and near-IR solar spectrum.

## *Experimental*

*Preparation and Characterization of the $TiO_2$ Electrode*: The fluorine-doped $SnO_2$ conducting glass (Hartford Glass) was cut in 20 mm × 30 mm rectangular pieces, and cleaned with ethanol (95%), distilled water, and ethanol (99.5%) in an ultrasonic bath for one hour in each case. A transparent film made of 20 nm particle $TiO_2$ paste was printed by doctor-blading on top of the conducting glass that was previously washed and dried. This paste was fabricated according to an acidic route in an autoclave [24]. The $TiO_2$-layer-coated glass was then heated to 450 °C for 30 min under oxygen for sintering. The film thickness was determined using a Dektak3 profilometer.

*Synthesis of Nanocrystalline $TiO_2$ Particles and Preparation of the Suspensions for the Multilayer Structure*: Nanocrystalline $TiO_2$ particles were synthesized by using a procedure reported by Burnside et al., based on the hydrolysis of titanium isopropoxide followed by a peptization process under hydrothermal conditions [25], which was slightly modified. In our case, 20 mL of titanium isopropoxide (97% Aldrich) were added to 36 mL of MilliQ water and stirred for one hour. Once the alcoxide was hydrolyzed, the product was filtered using 1.2 μm RTTP Millipore membranes, washed several times with distilled water, and placed in a Teflon reactor with 3.9 mL of an aqueous solution 0.6 M of tetramethylammonium hydroxide (Fluka). After homogenizing the suspension with a stirring bar, the reactor was placed in an oven preheated at 120 °C, where it was kept for three hours. A colloidal suspension of titanium oxide crystallites with an anatase structure, as confirmed by X-ray diffraction, was obtained. Later, centrifugation at 14 000 rpm (rpm: revolutions per minute) for 10 min allowed some large aggregates to be eliminated from the dispersion. A narrow distribution of nanocrystals centered on 5 nm was achieved after this process, as confirmed by photocorrelation spectroscopy and transmission electron microscopy. Silicon oxide nanoparticles (20 nm) were purchased from Dupont (LUDOX TMA colloidal silica, 34 wt.% suspension in $H_2O$). $TiO_2$ or $SiO_2$ nanoparticles were suspended in a mixture of water (21 vol. %) and methanol (79 vol. %) in order to be used as

precursors for the spin-coating process leading to the formation of the 1D PC within the cell.

*Fabrication and Structural Characterization of the Solar Cell Containing a 1D PC*: Before building the Bragg reflector onto the coated substrate, a layer of the above-mentioned fine titania particles was deposited by spin-coating in order to smooth the surface and obtain a uniform film. This last added layer was very thin compared to the titanium dioxide electrode. Then, in order to make the highly reflecting 1D PC, layers of silica and the same nc-TiO2 particles were deposited alternately by spin-coating 250 μL drops of their colloidal suspensions. For most cells, the titania-coated conducting substrate was spun at 100 rps. Periodic multilayers of different lattice parameters were attained by keeping the $TiO_2$ nanocrystal concentration constant at 5 wt. % and changing the silica concentration in the range 1–5 wt. % Alternatively, different rotation speeds between 100 and 150 rps were used to control the thickness of each layer in the multilayer. The PC properties of this structure were already evident to the naked eye after deposition of four layers, due to the high dielectric contrast between the two types of constituent layers. The refractive indices of the layers were estimated from fitting the optical properties to be $n_{SiO_2} = 1.24$, $n_{nc\text{-}TiO_2} = 1.74$, $n_{SiO_2} = 1.46$, and $n_{nc\text{-}TiO_2} = 2.03$ after electrolyte infiltration. For this work, six-layer stacks with lattice parameters of $120 \pm 10$ and $160 \pm 10$ nm were built, of which $85 \pm 5$ nm corresponded to the $TiO_2$ layer. After this, the multilayer-coated substrate was annealed at 450 °C in order to sinter the titania nanocrystals and remove all water bonded to the particles' surface. When the temperature reached 100 °C during the cooling process, the structure was removed from the furnace and immersed in a 0.5 mM solution of ruthenium bypiridile dye (N719, Dyesol) in ethanol overnight in order to assure proper adsorption of the dye on the nc-$TiO_2$ surface. The electrode was then rinsed with 99.5% ethanol for a few seconds. The counterelectrode was obtained after applying a 5 mM $H_2PtCl_6$ solution (Aldrich, 99.9%) in isopropanol (10 μL $cm^{-2}$) onto the conducting side and sintering in an oven for 30 min at 380 °C. A 45 μm thick hot-melt polymeric window (Surlyn, 1702 Dupont) previously cleaned overnight with 99.5% ethanol was placed on the counterelectrode and heated until the surlyn frame became attached to it. Afterwards, the electrodes were assembled and sealed by heating to 110 °C. Finally, they were put into electrical contact by filling the internal space between them with a liquid electrolyte using a vacuum pump. The employed electrolyte was composed of 100 mM $I_2$ (Aldrich, 99.999%), 100 mM LiI (Aldrich, 99.9%), 600 mM $[(C_4H_9)_4N]I$ (Aldrich, 98%), and 500 mM 4-tert-butylpyridine (Aldrich, 99%). The solvent used in this case was 3-methoxy propionitrile (Fluka, ≥99%). The porous nature of the periodic multilayer allowed the electrolyte to soak the sensitized nc-$TiO_2$ coating. Cross-sections of the cell were imaged using a field-emission scanning electron microscope (Hitachi 5200) operating at 5 kV and without using any conducting coating.

*Optical Reflection and Transmission Measurements*: Optical characterization was performed using a Fourier-transform IR spectrophotometer (BRUKER IFS-66) attached to a microscope and operating in reflection mode. A × 4 objective with a numerical aperture of 0.1 (light-cone angle ± 5.7°) was used to irradiate the solar cell and collect the reflected light at quasinormal incidence with respect to its surface. A spatial filter was used to selectively detect light from 1 $mm^2$ circular regions on the sample. The UV-vis transmission spectra were measured with a UV-vis scanning spectrophotometer (Shimadzu, UV-2101PC).

## Photoelectric Measurements

*J–V Characterization*: The devices under analysis were illuminated with a microwave-powered sulphur plasma lamp with a 1 sun equivalent (Lightdrive 1000, Fusion Lighting solar simulator, 1000 W $m^{-2}$ at 40 °C). A correction for the spectral mismatch between the simulated light and natural sunlight was made against a certified reference solar cell (IR-filtered silicon solar cell, Fraunhofer ISE, Freiburg, Germany). The DSSCs were masked to expose only the active area under all measurements. Incident-light intensities were adjusted with neutral wire-mesh attenuators. J–V curves were obtained by applying an external bias to the cell and measuring the generated photocurrent with a digital source meter (Keithley 2400). The voltage step and delay time of the photocurrent were approximately 8 mV ($V_{oc}$/100) and 1 s, respectively. The response of the cells to the angle of incidence of incoming light was analysed by mounting the cell onto a platform that could be tilted between 0° and 45°.

*IPCE Characterization:* The IPCE values were measured for solar cells in the UV-vis range (350–800 nm) of the electromagnetic spectrum. These measurements were obtained using a source meter (Keithley 2400), an autoranging picoammeter (Keithley 485), a 1/8 m monochromator (Spectral Products CM110), and a Xenon arc lamp (300W, ILC Technology, catalog no R300-5). An automatic filter wheel (AB 301, CM Instruments group) was used to remove second-order harmonics using cutoff filters for 400 nm radiation. The calibration was made against a certified reference solar cell (IR-filtered silicon solar cell, Fraunhofer ISE, Freiburg, Germany). The intensity was calibrated using a Newport optical power meter (model 1830-C) with a photodetector (818-UV). The incident monochromatic radiation was monitored in situ using a split-beam configuration. The controlling computer program was custom made and based on LabVIEW software.

## Acknowledgements

This work has been funded by the Ramón Areces Foundation, the Spanish Ministry of Science and Education, and the company Nanologica AB. We also acknowledge the Swedish Research Council and the Swedish Energy Agency. The DSSC coupled to 1D PCs is a concept protected by a US patent with serial number 61/046212. Supporting Information is available online from Wiley InterScience or from the author.

Received: December 14, 2007
Revised: June 20, 2008
Published online: December 16, 2008

[1] B. O'Regan, M. Grätzel, *Nature* **1991**, *353*, 737.
[2] M. Grätzel, *Inorg. Chem.* **2005**, *44*, 6841.
[3] A. Hagfeldt, M. Grätzel, *Acc. Chem. Res.* **2000**, *33*, 269.
[4] J. Bisquert, D. Cahen, G. Hodes, S. Ruhle, A. Zaban, *J. Phys. Chem. B* **2004**, *108*, 8106.
[5] K. Tennakone, G. R. R. A. Kumara, I. R. M. Kottegoda, V. P. S. Perera, *Chem. Comm.* **1999**, 15.
[6] P. Wang, C. Klein, R. Humphry-Baker, S. M. Zakeeruddin, M. Gratzel, *J. Am. Chem. Soc.* **2005**, *127*, 808.
[7] P. Wang, S. M. Zakeeruddin, J. E. Moser, E. Humphry-Baker, M. Grätzel, *J. Am. Chem. Soc.* **2004**, *126*, 7164.
[8] E. Palomares, J. N. Clifford, S. A. Haque, T. Lutz, J. R. Durrant, *J. Am. Chem. Soc.* **2003**, *125*, 475.
[9] M. Zukalova, A. Zukal, L. Kavan, M. K. Nazeeruddin, P. Liska, M. Gratzel, *Nano Lett.* **2005**, *5*, 1789.
[10] M. Law, L. E. Greene, J. C. Johnson, R. Saykally, P. Yang, *Nat. Mater.* **2005**, *4*, 455.
[11] S. A. Haque, E. Palomares, B. M. Cho, A. N. M. Green, N. Hirata, D. R. Klug, J. R. Durrant, *J. Am. Chem. Soc.* **2005**, *127*, 3456.
[12] A. Kay, M. Grätzel, *Sol. Energy Mater. Sol. Cells.* **1996**, *44*, 99.
[13] S. Ito, S. M. Zakeeruddin, R. Humphry-Baker, P. Liska, R. Charvet, P. Comte, M. K. Nazeeruddin, P. Péchy, M. Takata, H. Miura, S. Uchida, M. Grätzel, *Adv. Mater.* **2006**, *18*, 1202.
[14] D. C. Johnson, I. Ballard, K. W. J. Barnham, D. B. Bishnell, J. P. Connolly, M. C. Lynch, T. N. D. Tibbits, N. J. Ekins-Daukes, M. Mazzer, R. Airey, G. Hill, J. S. Roberts, *Sol. Energy. Mater. Sol. Cells* **2005**, *87*, 169.
[15] F. Llopis, I. Tobias, *Sol. Energy. Mater. Sol. Cells* **2003**, *87*, 481.
[16] L. Zeng, Y. Yi, C. Hong, J. Liu, N. Feng, X. Duan, L. C. Kimerling, B. A. Alamariu, *Appl. Phys. Lett.* **2006**, *89*, 1. *111*, 111.

[17] S. Nishimura, V. Abrams, B. A. Lewis, L. Halaoui, T. E. Mallouk, K. D. Benkstein, J. Lagemaat, A. J. Frank, *J. Am. Chem. Soc.* **2003**, *125*, 6306.
[18] S. Colodrero, M. E. Calvo, M. Ocaña, H. Míguez, *Langmuir* **2008**, *24*, 4430.
[19] A. Mihi, H. Míguez, S. Rubio, I. Rodríguez, F. Meseguer, *Phys. Rev. B: Condens. Matter* **2005**, *71*(125), 131.
[20] A. Mihi, H. Míguez, *J. Phys. Chem. B* **2005**, *109*, 15968.
[21] M. K. Nazeerudin, A. Kay, I. Rodicio, R. Humphry-Baker, E. Müller, P. Liska, N. Vlachopoulos, M. Grätzel, *J. Am. Chem. Soc.* **1993**, *115*, 6382.
[22] S. Södergren, A. Hagfeldt, J. Olsson, S. E. Lindquist, *J. Phys. Chem.* **1994**, *98*, 5552.
[23] P. G. O'Brien, N. P. Kherani, S. Zukotynski, G. A. Ozin, E. Vekris, N. Tetreault, A. Chutinan, S. John, A. Mihi, H. Míguez, *Adv. Mater.* **2007**, *19*, 4177.
[24] P. Wang, S. M. Zakeeruddin, P. Comte, R. Charvet, R. Humphry-Baker, M. Grätzel, *J. Phys. Chem. B* **2003**, *107*, 14336.
[25] S. D. Burnside, V. Shklover, C. Barbe, P. Comte, F. Arendse, K. Brooks, M. Grätzel, *Chem. Mater* **1998**, *10*, 2419.